Comparison of the removal efficiencies of Basic red 46 from aqueous solutions using Aşkale lignite with and without ultrasound assisted processes

Canan Karaca[a], Melike Karaca[a], Murat Kıranşan[b], Semra Karaca[a], Özkan Açışlı[a,*], Ahmet Gürses[c]

[a]*Department of Chemistry, Faculty of Science, Atatürk University, 25240 Erzurum, Turkey, email: ozkan.acisli@atauni.edu.tr*
[b]*Department of Chemistry and Chemical Processing Technologies, Gümüşhane Vocational School, Gümüşhane University, 29100 Gümüşhane, Turkey*
[c]*Department of Chemistry, K.K. Education Faculty, Atatürk University, 25240 Erzurum, Turkey*

ABSTRACT

This study compared the removal efficiencies of Basic red 46 from aqueous solutions with and without ultrasound-assisted processes using lignite as a low-cost adsorbent. The effects of various experimental parameters such as contact time, adsorbent dosage, initial solution, pH, initial dye concentration and temperature on the dye removal efficiency were investigated. The experimental results were modelled by the kinetic and isotherm models. Both of processes fitted well to pseudo-second-order kinetics and the Langmuir model with highest correlation coefficients for all of three temperatures. The results showed that the influence parameters have a different effect on the removal efficiency in the presence and absence of ultrasonic irradiation. When the results obtained for both processes are compared, it is seen that the removal efficiency obtained with the ultrasound assisted process is much higher than that obtained with non-ultrasound assisted process at high dye concentrations. The removal efficiency of ultrasound-assisted and unassisted processes was found to be 81.5% and 54.6%, respectively, at 80 mg/L dye concentration and 60 min. Thermodynamic parameters showed that the adsorption process was spontaneous and exothermic. The enthalpy and entropy changes for the ultrasound-assisted process were –9.35 kJ/mol and –0.03 kJ/K·mol, respectively.

Keywords: Basic red 46; Lignite; Adsorption; Ultrasound assisted process; Dye removal efficiency

1. Introduction

Many industries such as clothing, textile, leather, dyestuff, pharmaceutical, paper, plastic, food processing and cosmetic produce coloured effluents containing various pigments and dyes discharge the same to receiving waters [1,2]. From an environmental point of view, effluent streams containing the synthetic dyes even in trace quantities are highly undesirable because they have detrimental effects on photosynthetic phenomena by interfering the sunlight penetration. And also, some of them are toxic and carcinogenic properties. Therefore, dye removal from wastewaters is of great importance before releasing into the natural environment [1–4]. Most of the dyes are chemically stable and their biodegradability is low due to usually synthetic origin and complex molecular structure of them. In this case, their removal by applying conventional methods such as ozonation, chemical coagulation, electrochemical oxidation, photocatalytic discolouration is very difficult [1–4]. Adsorption has attracted attention as an effective, economic and feasible method and it has many advantages compared with the existing traditional treatment methods [1–7]. In addition to

* Corresponding author.

the use of activated carbons obtained from various precursors, leaf-based adsorbents and biochar for dye removal, chemical and photocatalytic degradation processes are also becoming increasingly widespread. In addition, in recent years, there have been many studies on biochar in the removal of organic and inorganic pollutants [8–12].

Although activated carbon is commonly used as an effective adsorbent in the adsorption processes, its use has become limited due to some reasons such as the high cost, the need for regeneration and decreased activity after regeneration [2,5,6]. The low-cost natural adsorbent materials such as lignite have been employed in the removal of colour and organic pollutants from aqueous solutions [13–15]. Coals exhibit a variety of surface properties and hence adsorption properties depending on its original plant nature [16,17]. To improve the limitations of other applications such as high cost, ineffective for removal some pollutant, operation problems and produce toxic secondary pollutants [18] over the past decade, combined adsorption applications in wastewater treatment have been accepted to be an effective purification process to reduce traces of dyes and organic pollutants [3,19]. For this purpose, one of the innovate technologies used with adsorption is sonication and many research studied in this subject is available in the literature [3,17,19–22]. It is reported that the ultrasound irradiation cause to enhance the rate of chemical reactions and mass and heat transfer using cavitation occurred [17,19,22]. Cavitation is the phenomenon of the formation, growth and collapse of microbubbles or cavities occurring in an extremely short time interval in a liquid [19,23]. By the collapse of cavities, a high amount of energy is released. The collapse of bubbles leads to forming of the regions with local high pressure and temperature [16]. Ultrasound creates to increase in surface area by forming many micro-cracks on the solid surface with cavitation [3]. As a result of water pyrolysis in the collapsing cavitation bubbles, hydroxyl ($^\bullet$OH) and hydrogen ($^\bullet$H) radicals are formed [3,18,22,23]. Then, they carried out the oxidation of the dissolved organic compounds by passing through into water with the result of the production of oxygen gas and hydrogen peroxide [3,18,23]. The reaction of volatile or hydrophobic compounds occurs both OH radicals and direct pyrolysis in the formed hot spots and interface by collapsing bubbles formed [18,22,23]. Although ultrasound

irradiation applications have different advantages, the fact that the degradation rates of many organic pollutants are too low for practical use can be seen as a disadvantage. One of the methods applied to solve this problem is the addition of solid particles or reagents [17–23]. Thus, degradation of the organic pollutants using this method will be carried out in shorter time and consequently the required time, energy and cost will be reduced. This study, it was aimed to compare the removal efficiencies of Basic red 46 from aqueous solutions with and without ultrasound-assisted processes, using lignite as a low-cost adsorbent. The influencing parameters on the dye removal process, such as initial Basic red 46 (BR 46) concentration, pH of the solution, lignite dose, temperature and time has been studied. The experimental results were evaluated by applying them to both the kinetic and isotherm models.
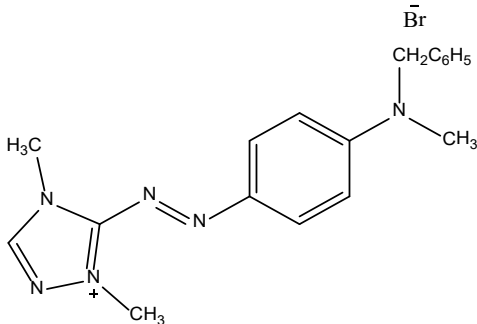
2. Materials and methods

2.1. Material

The low bituminous coal samples used as an adsorbent in this study were obtained from Aşkale coal mines in Turkey. The obtained samples were air-dried, ground and then sieved using ASTM standard sieves to give a fraction having a mesh size of −180 + 400. The Basic red 46 cationic dye used as adsorbate was obtained from Shimi Boyakhsaz Company (Iran) and used without purification. Table 1 shows the molecular structure and specific characteristics of dye. All other chemicals used in this study were analytical grade and provided by Sigma-Aldrich (Germany) Distilled water was used in the preparation of the solutions and all experimental work.

2.2. Experimental procedure

Batch adsorption experiments were performed in 150 mL glass-stoppered, round-bottom flasks immersed in a temperature-controlled thermostatic shaker at the constant stirring rate (150 rpm) and temperature (20°C) in neutral pH of 7. In ultrasonic-assisted adsorption experiments, ultrasonic irradiation was performed using a Bandelin SONOREX device (Germany, 40 kHz and 640 W) under the same experimental conditions. For this, first a 15-min adsorption process

Table 1
Molecular structure and specific characteristics of Basic red 46

C.I. name	Chemical structure	Molecular formula	M_w (g/mol)	λ_{max} (nm)
Basic red 46		$C_{18}H_{21}N_6Br$	401.3	530

was carried out and then ultrasonic irradiation was applied for a certain period of time. To ensure uniform conditions, the bottom of the flasks was kept fixed at a distance of 1.0 cm from the ultrasonic radiation source in all processes. A stock dye solution of 1000 mg/L was prepared with distilled water. Afterwards, experimental solutions were obtained at the desired concentration by diluting with distilled water. For use in the experiments, 0.1 g of lignite sample was mixed with 100 mL of the aqueous solutions of the various initial concentrations of BR 46. The various operational parameters such as time (5, 10, 20, 30, 40 and 60 min), temperature (293, 313 and 333 K), initial dye concentration (10, 20, 40, 60, 80 and 100 mg/L) and pH of the solution (3, 4, 6, 7, 8, 10 and 12) were selected and their effects on adsorption were examined. The pH of the solution was adjusted with concentrated HCl and NaOH solution by using a WTW inoLab pH meter (WTW Inc., Weilheim, Germany) with a combined pH electrode. In the adsorption experiments, the stirring speed of the thermostatic shaker was kept constant at 150 min⁻¹. At the end of each adsorption period, the samples were immediately centrifuged and the remaining dye concentration in solution was measured using the Varian Cary 100 UV-Vis Spectrophotometer (Australia) at a maximum wavelength of 530 nm. The dye removal percentage was calculated using Eq. (1):

$$\text{Removal}(\%) = \frac{(C_0 - C_t)}{C_0} \times 100 \tag{1}$$

where C_0 (mg/L) and C_t (mg/L) are the initial dye and dye concentrations at time t, respectively. The adsorbed dye amount q (mg/g) was calculated using Eq. (2):

$$q = \frac{(C_0 - C_e) \times V}{m} \tag{2}$$

where C_0 (mg/L) and C_e (mg/L) are the initial and equilibrium dye concentrations, respectively, V (L) is the volume of the solution and m (g) is the mass of the adsorbent.

3. Results and discussion

3.1. Characterization of lignite sample

3.1.1. Chemical composition and basic physical properties

The proximate and ultimate analyses results of the Aşkale lignite used in this study are given in Table 2 [14,24].

3.1.2. Mineralogical analysis

The mineralogical composition of Aşkale lignite was determined by X-ray diffraction spectroscopy and is given in Fig. 1. The main impure minerals found in lignite are quartz, pyrite, calcite and zeolite. It also contains a high proportion of the pyrite mineral with lignite [25]. A sharp peak at 26.66° and peaks at 39.48° and 43.28° seen in Fig. 1 indicate the presence of carbon-based microcrystalline graphite structures and aromatic layers in lignite.

3.1.3. Fourier-transform infrared spectroscopy analysis

The Fourier-transform infrared (FTIR) spectra of the raw Aşkale lignite, pure BR 46 cationic dye and the sample after adsorption at 293 K and the sample after ultrasonic irradiation are given in Fig. 2. The FTIR spectrum of coal and

Table 2
Proximate and ultimate analyses of the Aşkale lignite

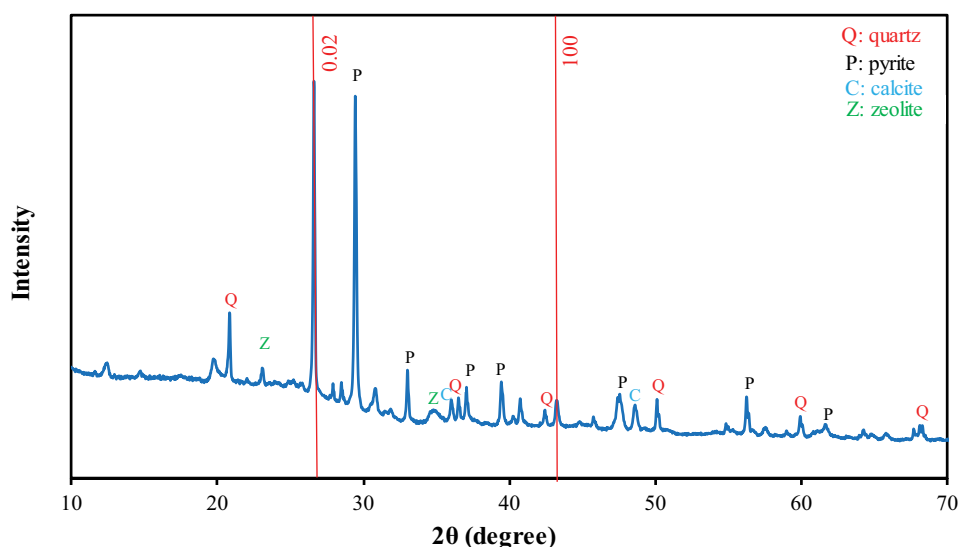| Moisture	Ash	Volatile matter	Fixed carbon	Carbon	Hydrogen	Sulfur	Nitrogen	Oxygen
4.46	29.64	34.28	31.62	70.86	4.28	4.76	2.20	17.90

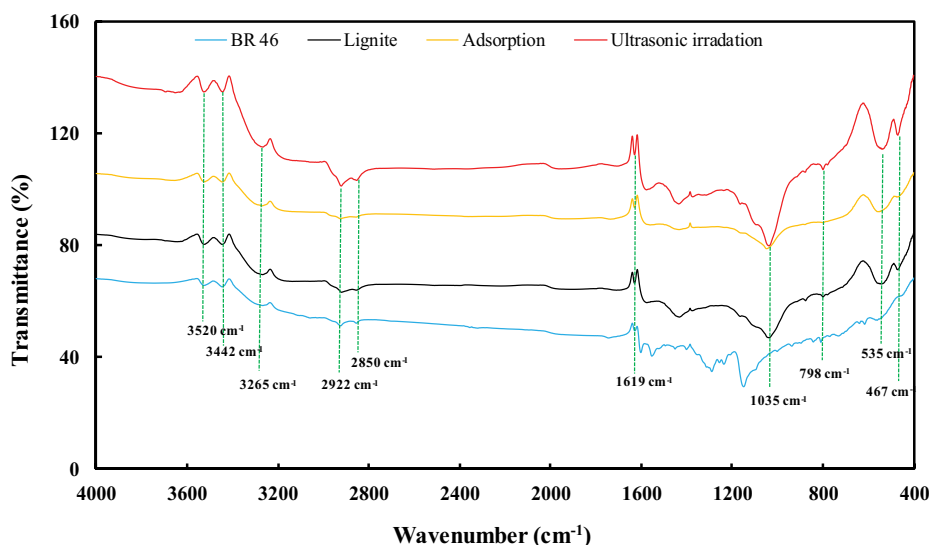Fig. 1. X-ray diffraction pattern of Aşkale lignite.

Fig. 2. Fourier-transform infrared spectra of the raw Aşkale lignite, pure BR 46 cationic dye and the sample after adsorption at 293 K and the sample after ultrasonic irradiation.

its derivatives can be broadly divided into four regions, respectively: aromatic structures at 900–700 cm^{-1}; groups containing oxygen at 1800–1000 cm^{-1}; aliphatic structures 3000–2800 cm^{-1}; hydrogen bonding sites at 3700–3000 cm^{-1} [26,27]. The bands at 467 and 525 cm^{-1} show Si–O–Si and Si–O–Al groups in the clay structure, respectively [28]. The band at 798 cm^{-1} represents the bending vibrational region of –CH outside the aromatic ring [29]. The absorption peak at 1619 cm^{-1} is attributed to C=C groups and 1035 cm^{-1} is assigned to the C–O stretching vibration as carbonyl groups [29]. The absorption peak around 2922 and 2850 cm^{-1} is due to the stretching vibration of –CH$_2$ and –CH$_3$ groups [29]. A sharp band around 3520 and 3442 cm^{-1} in the 3200–3600 cm^{-1} spectral region corresponds to overlapping symmetrical (H–O–H) and asymmetrical (H–O–H) stretch vibrations [28,30]. The symmetrical and asymmetrical bands of H–OH can be attributed to the water in the clay structure [28]. In addition, the C=N vibration peaks at 1675–1500 cm^{-1} and the C–H vibration peaks at 1250 cm^{-1} are also characteristic for the BR 46 dye. While these peaks are not visible in the lignite spectrum, they can be seen in the samples after adsorption and ultrasonic irradiation, which clearly demonstrates the adsorption of the dye by the lignite (Fig. 2).

3.1.4. Microstructural analysis

The scanning electron microscopy (SEM) technique is widely used to determine the surface morphology of the studied materials [31]. SEM images of Aşkale lignite at four different magnifications, together with the results of energy-dispersive X-ray spectroscopy (EDS) analysis are given in Fig. 3. It can be seen from these images that the lignite has a heterogeneous structure and exhibits a rough, non-porous but layered morphology. Furthermore, the EDS analysis results show very high oxygen and relatively high iron content. The high oxygen content means that the surface of the low-rank and high-ash lignite sample is highly oxidized and therefore contains a high percentage of oxy

functional groups as well as metal oxides. Both oxy-functional groups and metal oxide surfaces are highly favorable for cationic dye adsorption.

3.1.5. Surface area and pore structure of lignite

The specific surface area of lignite was measured on a Micromeritics 3 Flex Instrument (USA) using nitrogen adsorption–desorption isotherms at –197.2°C with relative pressure varying from 0 to 1. Before measurements, the lignite sample was degassed for 1.5 h at 100°C in the degassing port of the adsorption analyser. In this stage, the total pore volume of the sample was measured for the single point P/P^0 value of 0.988, and the pore size distribution was determined by the Barrett–Joyner–Halenda (BJH) method.

From the values in Table 3, it can be said that lignite has low porosity and mesopores [32]. Fig. 4 shows the N$_2$ adsorption/desorption Brunauer–Emmett–Teller (BET) isotherm of lignite and reflects the Type-II isotherm and H$_4$ hysteresis loop according to the isotherm The International Union of Pure and Applied Chemistry (IUPAC) classification. This type of isotherm indicates strong interactions between adsorbate and adsorbent and multilayer adsorption [14,33]. In addition, the physical absorption of most gases on non-porous or macroporous adsorbents can also conform to the reversible Type II isotherm [33]. It can be seen from the same table that the BET (N$_2$) surface area and monolayer adsorption capacity are 20.27 m^2/g and 11.44 cm^3/g, respectively. The mean pore diameter and total pore volume are also 4.041 nm and 0.021 cm^3/g, respectively. Coals with mesoporous structures containing open slit-shaped capillaries with a wide body and narrow short neck may exhibit an H$_4$ hysteresis ring [14]. H$_4$ hysteresis loops are generally observed in aggregated zeolite crystals, microporous carbons and some porous zeolites [33]. The results obtained from the X-ray diffraction spectra and SEM images of lignite are also in line with these results.

Fig. 5 shows the pore size distribution of the lignite sample based on the BJH model. From this figure, it can
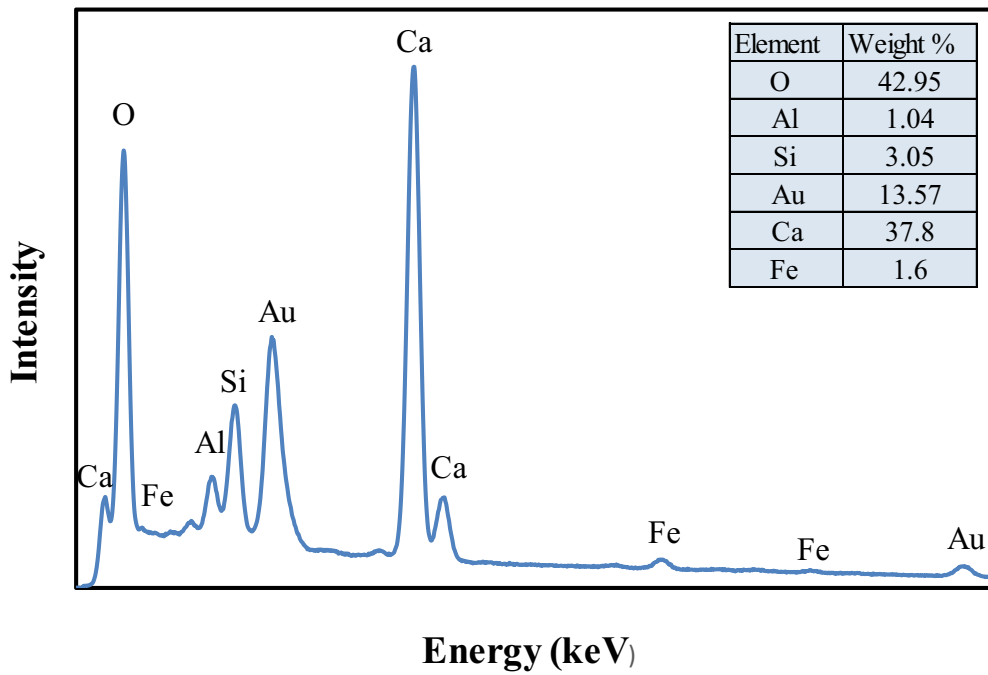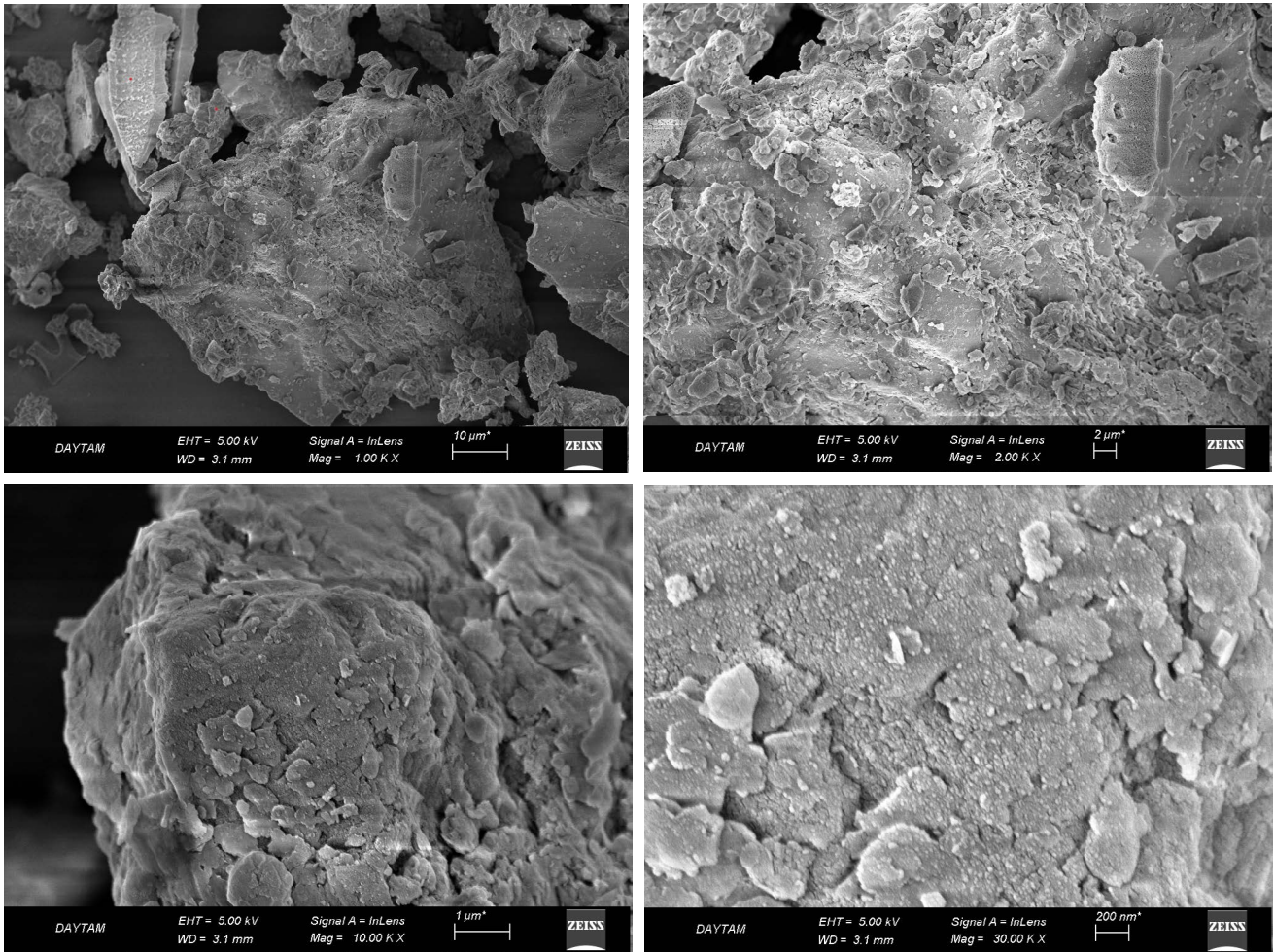
Fig. 3. Scanning electron microscopy images and energy-dispersive X-ray spectra of Aşkale lignite.

Table 3
Results of the surface area measurements of lignite

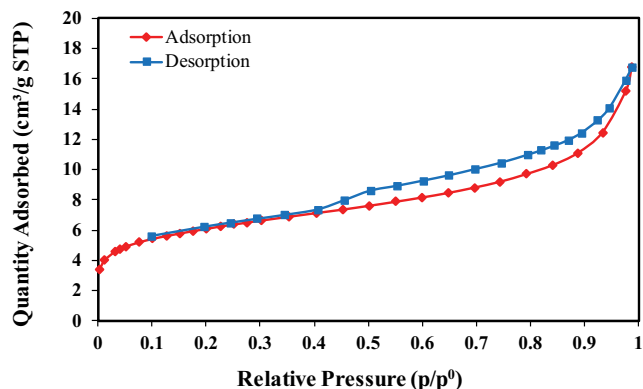| Parameter	Lignite
Brunauer–Emmett–Teller surface area (m^2/g)	20.72
Barrett–Joyner–Halenda cumulative surface area (m^2/g)	11.44
Total pore volume (cm^3/g)	0.021
Average pore width (nm)	4.041

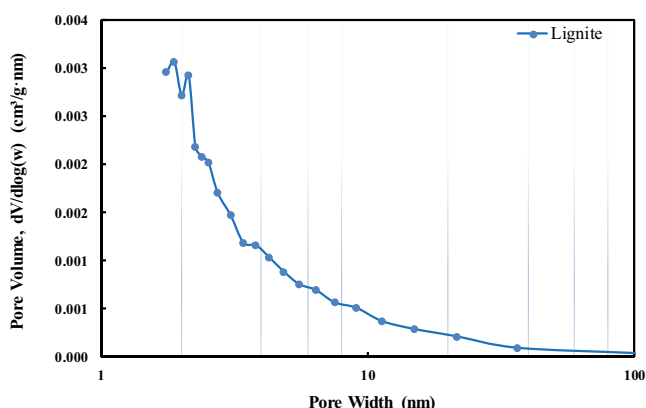Fig. 4. Isotherms of N$_2$ adsorption/desorption of Aşkale lignite.

Fig. 5. Barrett–Joyner–Halenda pore-size distribution of the Aşkale lignite.

be seen that the pore volume size distribution of the lignite sample is mainly in particles finer than 10 nm.

3.2. Operational parameter

3.2.1. Effect of adsorbent dosage

To examine the effect of adsorbent dosage on the removal efficiency of BR 46, adsorption experiments with and without ultrasonic radiation were carried out at 293 K temperature, natural pH 80 mg/L initial dye concentration and various adsorbent dosages between 0.25 and 1.00 g/100 mL for 30 min. The results are plotted in Fig. 6a and b.

From Fig. 6a and b, it can be seen that in both ultrasound-assisted and unassisted adsorption experiments, the adsorbed amount is relatively low but the removal efficiency
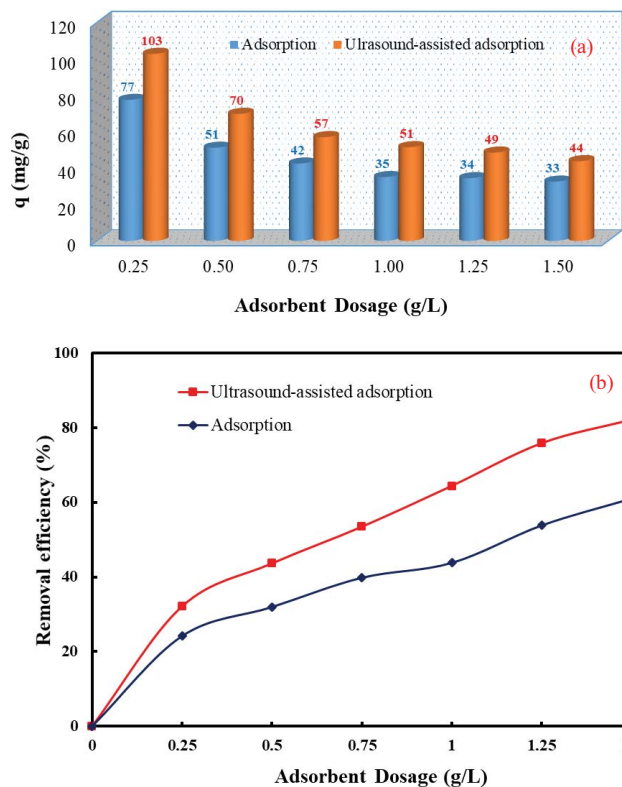

Fig. 6. (a) Effect of adsorbent dosage on adsorbed dye amount onto lignite without and with ultrasound-assisted ([BR 46]$_0$: 80 mg/L, temperature: 293 K, and contact time: 30 min). (b) Effect of adsorbent dosage on the dye removal efficiency by adsorption onto lignite without and with ultrasound-assisted ([BR 46]$_0$: 80 mg/L, temperature: 293 K and contact time: 30 min).

increases with increasing adsorbent dosage. The trend of change in the adsorbed amounts can be explained by the fact that the adsorbate amount does not increase at the same ratio with the increasing amount of adsorbent, depending on the adsorbed amounts calculated as per unit adsorbent. For this reason, the adsorbent dosage was taken as 0.10 g/100 mL in all other experiments. The fact that the rate of change of adsorption efficiency is lower with increasing adsorbent dosage in the non-ultrasonic-assisted process, that is, the curve has a lower slope, can be explained by the relative decrease in the density of sites suitable for adsorption due to aggregation and therefore the decrease in the total surface area can be used and is the relative extension of the diffusion path length [19,34]. The relative increase observed in the values obtained from ultrasound-assisted experiments can be attributed to the decrease in diffusion resistance due to disaggregation or cavitation induced by radiation.

However, it is highly probable that cavitation will create microcracks in the lignite structure, resulting in a higher surface area, and also increase the effectiveness of the radicals generated by ultrasound irradiation in dye removal.

3.2.2. Effect of initial dye concentration

The variation of the adsorption capacity with time was investigated as non-ultrasound-assisted and ultrasound-

assisted, and the results are given in Fig. 7a and b, respectively, for various initial dye concentrations. It can be seen from Fig. 7a that the time to reach adsorption equilibrium is approximately 10 min for all initial concentrations. In ultrasound-assisted experiments, it can be seen from Fig. 7b that while the time to reach equilibrium is 10 min at low initial dye concentrations, the time increases up to about 30 min in higher dye concentrations. However, the removal efficiencies obtained at all initial dye concentrations in ultrasound-assisted experiments were higher than those obtained from experiments without ultrasound-assisted. Accordingly, it can be said that the dye removal at low concentrations is not very dependent on the type of process and the adsorption capacity of lignite is high enough. However, at higher dye concentrations, the removal and increase in time observed in ultrasound-assisted experiments is due to increased mass and heat transfer due to a possible temperature increase by adiabatic collapse of microbubbles as a result of moisture evaporation, and changes in the textural structure of lignite with partial removal of volatile matter and sulfur via thermal decomposition. as well as increased interactions between dye molecules and hydroxyl or other radicals [18,23,35,36]. Hydrogen peroxide, which can form in the aqueous environment during the degradation of the dye, can also change the surface and textural properties of lignite [3,18,23].

It has also been reported that degradation of lignite by hydrogen peroxide can lead to residue rich in aliphatic compounds and carboxylic groups [37].

3.2.3. Effect of pH

The pH of the solution has a critical role in adsorption since it can affect the properties of both adsorbent and adsorbate, and also plays a role in the generation of reactive radicals [22,34]. The dependence of the removal efficiency of BR 46 with and without ultrasound assisted processes on the initial pH of the solution was investigated in the pH range of 3–12. In the experiments initial dye concentration was fixed to be 10 mg/L, the adsorbent dosage was 1 g/L and the temperature was 293 K. The results were presented in Fig. 8. As shown in Fig. 8, pH has not significantly affected in both two processes. From Fig. 8, in which the results obtained are graphed, it can be seen that with the increase of solution pH, the removal efficiency first decreases slightly and then increases. However, the removal efficiency in the ultrasound assisted process is much higher than in the non-ultrasound assisted process at all pHs studied. Especially in the pH range of 4.0–8.0, the adsorption of cationic dye will be partially reduced due to possible protonation of carboxylic and phenolic groups on the lignite surface [38]. However, the removal efficiency increased due to the possible opposite change in surface charge with increasing hydroxyl ion concentration, as well as the effectiveness of interactions such as hydrophobic and/or hydrogen bonding. The increases observed in the dye removal efficiency in the ultrasound-assisted process indicate the positive effect of the presence of radical species. Thus, it can be said that ultrasonic irradiation causes both the degradation of dye molecules by radicals and an increase in active adsorption sites in the adsorbent as a result of cavitation. Merouani et al. [39] reported that the sonochemical dissociation of Rhodamine B at very low pH was higher than that obtained at higher pH.

3.2.4. Effect of temperature

The variation of dye removal efficiency by non-ultrasound-assisted and ultrasound-assisted processes with
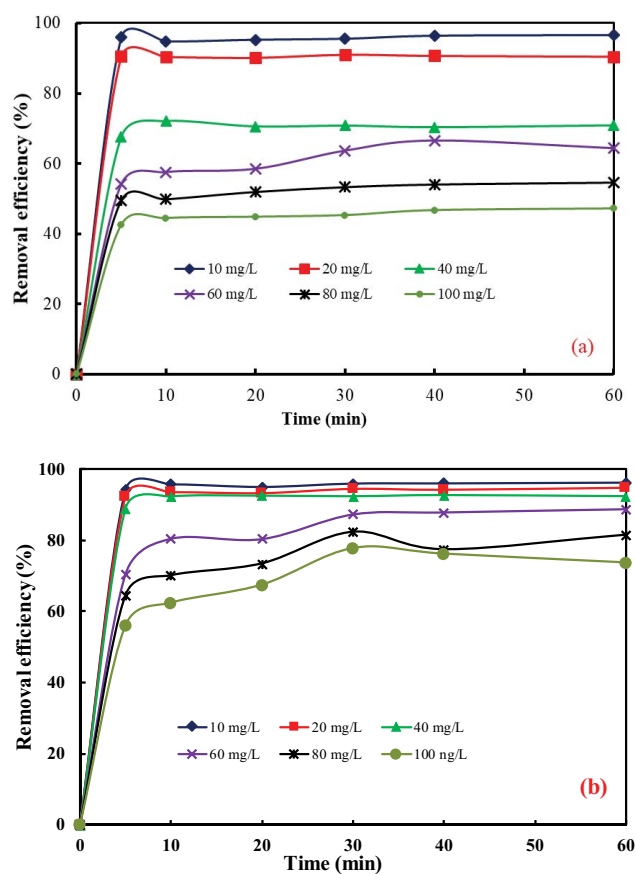

Fig. 7. Variation of dye removal efficiency with contact time at different initial dye concentrations for non-ultrasound-assisted process (a) and ultrasound-assisted process (b) (adsorbent dosage: 0.1 g/100 mL, and temperature: 293 K).
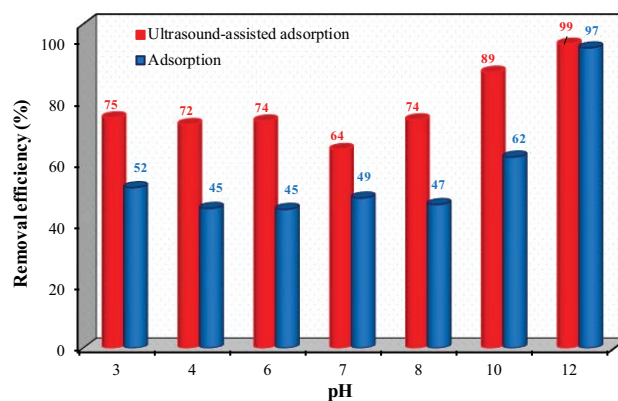

Fig. 8. Variation of dye removal efficiency with initial solution pH for both non-ultrasound-assisted and ultrasound-assisted processes (contact time: 30 min, temperature: 293 K, adsorbent dosage: 0.1 g/100 mL and [BR 46]$_0$: 80 mg/L).

temperature (293, 313 and 333 K) was investigated as a function of contact time, and the results are plotted in Fig. 9a and b, respectively. From both figures, it can be seen that the dye removal increases with increasing temperature, but the increase is higher in the ultrasonic assisted process. Accordingly, it can be said that the adsorption process is endothermic in nature and that the temperature increase positively affects both radical species formation and radical interactions. This can be explained by the thermal movement increasing with temperature and the dominant effect of hydroxyl radicals in the degradation of the dye [40].

3.3. Isotherm studies

Examining the compatibility of experimental data with isotherm models is very important in terms of elucidating the adsorption mechanism [20,21]. For this, the compatibility of the results obtained from the experiments with non-ultrasound assisted and ultrasound assisted processes at 293 K to the most widely used isothermal models such as Langmuir, Freundlich, Temkin, Dubinin–Radushkevich, Harkins–Jura, BET, Halsey, and Smith & Henderson were examined. For this, the constants related to the models were calculated by linear regression using linear forms of the isotherm equations and are given in Table 4 together with the regression coefficients and isotherm equations with only relatively
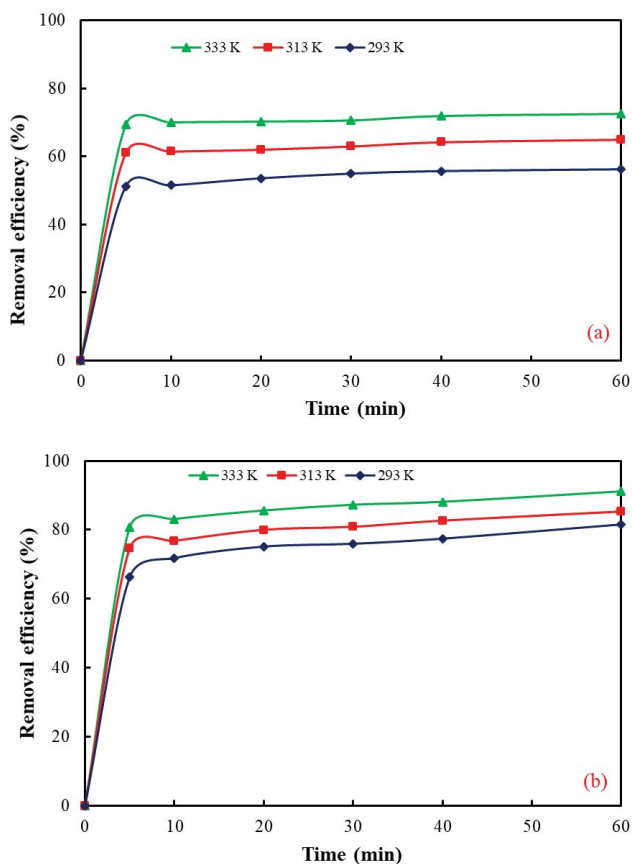
high fit. Therefore, the table does not include relevant results from BET, Halsey and Smith & Henderson isotherm models. It can be seen from Table 4 that the highest agreement of experimental data for both processes is obtained with the Langmuir model. Accordingly, it can be said that a homogeneous, monolayer, localized adsorption takes place on active sites with equal energy in both processes and the interaction between adsorbed particles is limited [41].

3.4. Kinetics studies

Investigation of adsorption kinetics is extremely important in terms of determining the rate and mechanism of adsorption and thus being able to design the system. Therefore, in this study, the experimental data obtained from the experiments with non-ultrasound assisted and ultrasound assisted processes at 293, 313 and 333 K, has been applied to kinetic models such as pseudo-first-order, pseudo-second-order, intraparticle diffusion and Elovich [24]. Equations of these kinetic models are given in Eqs. (3)–(5), respectively [42–47].

$$\ln\left(q_e - q_t\right) = \ln q_e - k_1 t \tag{3}$$

$$\frac{t}{q_t} = \frac{1}{k_2 q_e^2} + \frac{t}{q_e} \tag{4}$$

$$q_t = k_i \sqrt{t} + C \tag{5}$$

where q_e and q_t are the amounts of BR 46 adsorbed at equilibrium and at a given time, respectively, k_1 (s^{-1}) is the rate constant of the pseudo-first-order model, k_2 (g/mg·s) is the rate constant of the pseudo-second-order model, (mg/s$^{1/2}$·g), k_i is the intraparticle diffusion rate constant and C (mg/g) is the boundary layer thickness [42–44].

For this purpose, the constants calculated from the linear regression analysis of the curves resulting from the application of the experimental data to the linear forms of the kinetic equations, together with the regression coefficients and kinetic equations, are given in Table 5. It can be seen from Table 5 that the kinetic data from experiments with both processes can be well described to the pseudo-second-order kinetic model, with the highest R^2 values. Thus, in parallel with the isotherm analysis results, it can be argued that the interactions between the dye particles and the active groups on the lignite surface are highly effective, and that the chemical interaction of the dye with the radical species plays a decisive role in dye removal.

3.5. Thermodynamic studies

The changes in thermodynamic quantities such as isostatic enthalpy ($\Delta H°_{ads}$), isostatic entropy ($\Delta S°_{ads}$) and Gibbs free energy ($\Delta G°_{ads}$) for BR 46 adsorption on lignite by ultrasound assisted process were calculated using the equations given in Eqs. (8)–(10) [48]:

$$\frac{d\left(\ln C\right)}{d\left(1/T\right)} = -\frac{\Delta H_{ads}}{R} \tag{6}$$

Fig. 9. Effect of temperature on the dye removal for non-ultrasound-assisted process (a) and ultrasound-assisted process (b) ([BR 46]$_0$: 80 mg/L, pH: 6.2, and adsorbent dosage: 0.1 g/100 mL).

Table 4
Compatibility of the results obtained from the experiments with non-ultrasound assisted and ultrasound assisted processes at 293 K for 30 min

Isotherm	Equation	Parameters	Non-ultrasound assisted process	Ultrasound-assisted process
			293 K	293 K
Langmuir	$C/q = 1/Kq_m + (1/q_m)C$	q_m	50.50	89.28
		K	0.14	0.23
		R^2	0.988	0.990
Freundlich	$\ln q = \ln K_f + n\ln C$	n	0.12	0.51
		K_f	17.43	17.50
		R^2	0.859	0.981
Temkin	$q_e = (RT/b_T)\ln a_T + (RT/b_T)\ln C_e$	b_T	0.26	0.47
		a_T	2.42	3.40
		R^2	0.934	0.980
Dubinin–Radushkevich	$\ln q = K\varepsilon^2 + \ln q_{DR}$	K	−8.00E-07	−2.00E-07
		q_{DR}	37.91	52.39
		R^2	0.734	0.815
Harkins–Jura	$1/q^2 = (B/A) − (1/A)\log C$	B	1.60	1.05
		A	166.66	188.67
		R^2	0.496	0.714

q and q_e adsorption capacity of lignite (mg/g); q_m monolayer adsorption capacity (mg/g); C and C_e equilibrium concentration (mg/L); n, K, K_f, b_T, a_T, q_{DR}, B and A are constant parameters for the isotherm equations.

Table 5
Calculated parameters of the kinetic models for the results obtained from the experiments with non-ultrasound assisted and ultrasound assisted processes at 293 K

	Initial concentration	Temp. (K)	Pseudo-first-order	Pseudo-second-order				Intraparticle diffusion		
			R^2	k_2	$q_{e,exp}$	$q_{e,cal}$	R^2	k_{in}	C	R^2
	mg/L			g/mg·s	mg/g	mg/g		mg/s$^{1/2}$·g		
	10	293	0.0236	–	8.2437	8.6730	0.9965	–	9.6752	0.4683
	20	293	0.3031	–	18.3907	18.2815	0.9999	0.0039	18.2430	0.1934
	40	293	0.2907	0.00795	28.3172	28.2486	0.9996	0.0129	27.7110	0.1378
Non-ultrasound assisted process	60	293	0.6785	0.00027	38.1838	40.0000	0.9980	0.1515	32.2180	0.9002
	80	293	0.4893	0.00038	42.6306	44.2478	0.9998	0.0920	39.1920	0.9251
	100	293	0.2795	0.00037	45.2611	47.6190	0.9996	0.0915	42.5820	0.9746
	80	313	0.2936	0.00042	50.3926	52.3560	0.9997	0.0669	48.3600	0.9112
	80	333	0.1307	0.00054	56.4429	58.1395	0.9998	0.0513	55.1440	0.8975
	10	293	0.022	0.01138	9.6093	9.6525	1.0000	0.0039	9.4564	0.7978
	20	293	0.1009	0.00401	18.8897	19.0114	1.0000	0.0097	18.4750	0.9074
	40	293	0.0229	0.00536	36.9807	37.0370	1.0000	0.0251	36.0790	0.6119
Ultrasound assisted process	60	293	0.7139	0.00018	52.4333	54.9451	0.9994	0.2271	43.2260	0.9403
	80	293	0.7789	0.00014	65.8781	66.6667	0.9977	0.2845	51.9700	0.8548
	100	293	0.5583	0.00012	77.8143	77.5194	0.9961	0.4364	56.7610	0.8369
	80	313	0.4905	0.00018	64.6750	68.9655	0.9993	0.1692	59.2720	0.9609
	80	333	0.5531	0.00019	69.7679	73.5294	0.9994	0.1630	64.1890	0.9682

$$\frac{d(\ln C)}{d(\ln T)} = \frac{\Delta S_{ads}}{R} \quad (7)$$

$$\Delta G^\circ = -RT\ln K \quad (8)$$

where C is the equilibrium dye concentration (mg/L), T is the absolute temperature (K) and R is the gas constant (8.314 × 10^{-3} kJ/mol·K). The results are summarized in Table 6. As can be seen from Table 6, ΔH°_{ads} has positive values, ΔG°_{ads} and ΔS°_{ads} have negative values. With increasing

Table 6
Calculated thermodynamic parameters for BR 46 adsorption on lignite by ultrasound assisted process

Adsorbent	T (K)	C (mg/L)	q (mg/g)	$\Delta G°$ (kJ/mol)	ΔH_{ads} (kJ/mol)	ΔS_{ads} (kJ/K·mol)
Lignite (C_0: 80 mg/L)	293	37.37	42.63	–27.31		
	313	29.61	50.39	–30.57	–9.35	–0.03
	333	23.56	56.44	–34.51		

temperature, the amount of adsorbed dye (q) also increases, indicating that the process is endothermic. In addition, the negative $\Delta G°_{ads}$ values calculated for all temperatures mean that the ultrasound assisted process occurs spontaneously [49]. On the other hand, negative entropy values mean a decrease in disorder after adsorption and this can be associated with the dispersion of water molecules that surround dye ions in bulk phase and form a regular structure after adsorption.

4. Conclusions

The removal of Basic red 46 from aqueous solutions by adsorption method using lignite, with and without ultrasonic radiation, was investigated. In ultrasonic radiation-assisted treatment, it has been observed that, due to the effect of radicals produced by the cavitation process and increased mass transfer, the decolorization efficiency is quite high at high initial dye concentrations in the range of 60–100 mg/L. From the examination of the fit of experimental data to various isotherm models, it was seen that the best fit for all temperatures in both processes was obtained with the Langmuir adsorption model (R^2: 0.988, q_m: 50.50 mg/g non-ultrasound assisted process and R^2: 0.990, q_m: 89.28, ultrasound-assisted process). Examination of the fit of experimental data to kinetic models also showed that the best fit was obtained with the pseudo-second-order model in both processes (R^2: 0.999 at all initial concentrations). From thermodynamic studies, isosteric adsorption enthalpy and entropy were calculated as –9.35 kJ/mol and –0.03 kJ/K·mol, respectively. Accordingly, it can be said that lignite can be used effectively as a low-cost natural adsorbent in dye removal from aqueous solutions and ultrasonic assisted adsorption process can also be an effective alternative treatment method.

Acknowledgements

References

[1] K.G. Bhattacharyya, A. Sarma, Adsorption characteristics of the dye, Brilliant Green, on Neem leaf powder, Dyes Pigm., 57 (2003) 211–222.

[2] R. Darvishi Cheshmeh Soltani, A.R. Khataee, M. Safari, S.W. Joo, Preparation of bio-silica/chitosan nanocomposite for adsorption of a textile dye in aqueous solutions, Int. Biodeterior. Biodegrad., 85 (2013) 383–391.

[3] E. Şayan, M.E. Edecan, An optimization study using response surface methods on the decolorization of Reactive Blue 19 from aqueous solution by ultrasound, Ultrason. Sonochem., 15 (2008) 530–538.

[4] A. Kurniawan, H. Sutiono, N. Indraswati, S. Ismadji, Removal of basic dyes in binary system by adsorption using rarasaponin-bentonite: revisited of extended Langmuir model, Chem. Eng. J., 189 (2012) 264–274.

[5] D.K. Mahmoud, M.A.M. Salleh, W.A.W.A. Karim, A. Idris, Z.Z. Abidin, Batch adsorption of basic dye using acid treated kenaf fibre char: equilibrium, kinetic and thermodynamic studies, Chem. Eng. J., 181 (2012) 449–457.

[6] W. Zhang, H. Li, X. Kan, L. Dong, H. Yan, Z. Jiang, H. Yang, A. Li, R. Cheng, Adsorption of anionic dyes from aqueous solutions using chemically modified straw, Bioresour. Technol., 117 (2012) 40–47.

[7] B. Cojocariu, A.M. Mocanu, G. Nacu, L. Bulgariu, Possible utilization of PET waste as adsorbent for Orange G dye removal from aqueous media, Desal. Water Treat., 104 (2018) 338–345.

[8] S. Praveen, J. Jegan, T. Bhagavathi Pushpa, R. Gokulan, L. Bulgariu, Biochar for removal of dyes in contaminated water: an overview, Biochar, 4 (2022) 10, doi: 10.1007/s42773-022-00131-8.

[9] S. Majidian, M. Taghavi, N. Afshar Kohan, A. Dehghan, M. Afsharnia, Photocatalytic degradation of methylene blue dye using bismuth oxyiodide from aqueous solutions, Int. J. Environ. Anal. Chem., (2022), doi: 10.1080/03067319.2021.2014463.

[10] M. Afsharnia, H. Biglari, A. Javid, F. Zabihi, Removal of Reactive Black 5 dye from aqueous solutions by adsorption onto activated carbon of grape seed, Iran. J. Health Sci., 5 (2017) 48–61.

[11] L. Bulgariu, L.B. Escudero, O.S. Bello, M. Iqbal, J. Nisar, K.A. Adegoke, F. Alakhras, M. Kornaros, I. Anastopoulos, The utilization of leaf-based adsorbents for dyes removal: a review, J. Mol. Liq., 276 (2019) 728–747.

[12] M.R. Samarghandi, M. Zarrabi, A. Amrane, M.N. Sepehr, M. Noroozi, S. Namdari, A. Zarei, Kinetic of degradation of two azo dyes from aqueous solutions by zero iron powder: determination of the optimal conditions, Desal. Water Treat., 40 (2012) 137–143.

[13] S. Karaca, A. Gurses, R. Bayrak, Effect of some pre-treatments on the adsorption of methylene blue by Balkaya lignite, Energy Convers. Manage., 45 (2004) 1693–1704.

[14] A. Gurses, A. Hassani, M. Kiransan, O. Acisli, S. Karaca, Removal of methylene blue from aqueous solution using by untreated lignite as potential low-cost adsorbent: kinetic, thermodynamic and equilibrium approach, J. Water Process Eng., 2 (2014) 10–21.

[15] M. Aivalioti, D. Pothoulaki, P. Papoulias, E. Gidarakos, Removal of BTEX, MTBE and TAME from aqueous solutions by adsorption onto raw and thermally treated lignite, J. Hazard. Mater., 207–208 (2012) 136–146.

[16] V.K. Gupta, Suhas, Application of low-cost adsorbents for dye removal—a review, J. Environ. Manage., 90 (2009) 2313–2342.

[17] M.H. Entezari, Z. Sharifalhoseini, Sono-sorption as a new method for the removal of methylene blue from aqueous solution, Ultrason. Sonochem., 14 (2007) 599–604.

[18] E. Şayan, Optimization and modeling of decolorization and COD reduction of reactive dye solutions by ultrasound-assisted adsorption, Chem. Eng. J., 119 (2006) 175–181.

[19] M. Roosta, M. Ghaedi, N. Shokri, A. Daneshfar, R. Sahraei, A. Asghari, Optimization of the combined ultrasonic assisted/

adsorption method for the removal of malachite green by gold nanoparticles loaded on activated carbon: experimental design, Spectrochim. Acta, Part A, 118 (2014) 55–65.

[20] M. Roosta, M. Ghaedi, M. Mohammadi, Removal of Alizarin Red S by gold nanoparticles loaded on activated carbon combined with ultrasound device: optimization by experimental design methodology, Powder Technol., 267 (2014) 134–144.

[21] M.Q. Cai, X.Q. Wei, Z.J. Song, M.C. Jin, Decolorization of azo dye Orange G by aluminum powder enhanced by ultrasonic irradiation, Ultrason. Sonochem., 22 (2015) 167–173.

[22] A. Khataee, M. Sheydaei, A. Hassani, M. Taseidifar, S. Karaca, Sonocatalytic removal of an organic dye using TiO$_2$/montmorillonite nanocomposite, Ultrason. Sonochem., 22 (2015) 404–411.

[23] M.R. Doosti, R. Kargar, M.H. Sayadi, Water treatment using ultrasonic assistance: a review, Proc. Int. Acad. Ecol. Environ. Sci., 2 (2012) 96.

[24] A. Gürses, S. Bayrakçeken, M.Ş. Gülaboğlu, Adsorption of o-cresol from aqueous solution on coal, Colloids Surf., 64 (1992) 7–13.

[25] Ö. AÇIŞLI, Değişik Gaz Atmosferlerinde Balkaya Linyitinin Desülfürizasyonu, Atatürk Üniversitesi, 2002.

[26] C.F. Wang, X. Fan, F. Zhang, S.Z. Wang, Y.P. Zhao, X.Y. Zhao, W. Zhao, T.G. Zhu, J.L. Lu, X.Y. Wei, Characterization of humic acids extracted from a lignite and interpretation for the mass spectra, RSC Adv., 7 (2017) 20677–20684.

[27] W. Zhang, S. Jiang, K. Wang, L. Wang, Y. Xu, Z. Wu, H. Shao, Y. Wang, M. Miao, Thermogravimetric dynamics and FTIR analysis on oxidation properties of low-rank coal at low and moderate temperatures, Int. J. Coal Prep. Util., 35 (2015) 39–50.

[28] Ş.B. 2 Ceyda BİLGİÇ, Application of Fourier Transform Infrared (FTIR) Spectroscopy to Analysis of Clays, Nevşehir Bilim ve Teknoloji Dergisi, 2019, pp. 37–46.

[29] X. He, X. Liu, B. Nie, D. Song, FTIR and Raman spectroscopy characterization of functional groups in various rank coals, Fuel, 206 (2017) 555–563.

[30] Ö. Açışlı, S. Karaca, A. Gürses, Investigation of the alkyl chain lengths of surfactants on their adsorption by montmorillonite (Mt) from aqueous solutions, Appl. Clay Sci., 142 (2017) 90–99.

[31] Ö. Açışlı, Doum Palm Meyve Kabuklarından Aktif Karbon Üretimi ve Karakterizasyonu, Avrupa Bilim ve Teknoloji Dergisi., 2019, pp. 544–551.

[32] O.P. Meyers (Ed.) by R.A. Meyers, Mahajan, Coal Structure, Elsevier, Academic Press, New York, London, 1982, pp. 51–86.

[33] M. Thommes, K. Kaneko, A.V. Neimark, J.P. Olivier, F. Rodriguez-Reinoso, J. Rouquerol, K.S.W. Sing, Physisorption of gases, with special reference to the evaluation of surface area and pore size distribution (IUPAC Technical Report), Pure Appl. Chem., 87 (2015) 1051–1069.

[34] N.M. Mahmoodi, F. Najafi, S. Khorramfar, F. Amini, M. Arami, Synthesis, characterization and dye removal ability of high capacity polymeric adsorbent: polyaminoimide homopolymer, J. Hazard. Mater., 198 (2011) 87–94.

[35] S. Karaca, Desulfurization of a Turkish lignite at various gas atmospheres by pyrolysis. Effect of mineral matter, Fuel, 82 (2003) 1509–1516.

[36] Z. Eren, Ultrasound as a basic and auxiliary process for dye remediation: a review, J. Environ. Manage., 104 (2012) 127–141.

[37] L. Doskočil, L. Grasset, D. Válková, M. Pekař, Hydrogen peroxide oxidation of humic acids and lignite, Fuel, 134 (2014) 406–413.

[38] S. Merouani, O. Hamdaoui, F. Saoudi, M. Chiha, Sonochemical degradation of Rhodamine B in aqueous phase: effects of additives, Chem. Eng. J., 158 (2010) 550–557.

[39] A. Gürses, S. Karaca, M. Açikyildiz, M. Ejder, Thermodynamics and mechanism of cetyltrimethylammonium adsorption onto clayey soil from aqueous solutions, Chem. Eng. J., 147 (2009) 194–201.

[40] M. Goel, H. Hongqiang, A.S. Mujumdar, M.B. Ray, Sonochemical decomposition of volatile and non-volatile organic compounds—a comparative study, Water Res., 38 (2004) 4247–4261.

[41] J.S. Cao, J.X. Lin, F. Fang, M.T. Zhang, Z.R. Hu, A new absorbent by modifying walnut shell for the removal of anionic dye: kinetic and thermodynamic studies, Bioresour. Technol., 163 (2014) 199–205.

[42] Y.S. Ho, G. McKay, Pseudo-second-order model for sorption processes, Process Biochem., 34 (1999) 451–465.

[43] S.K. Lagergren, About the theory of so-called adsorption of soluble substances, Sven. Vetenskapsakad. Handingarl., 24 1898.

[44] W.J. Weber, J.C. Morris, Kinetics of adsorption on carbon from solution, J. Sanit. Eng. Div., 89 (1963), doi: 10.1061/JSEDAI.0000430.

[45] V.V. Basava Rao, S. Ram Mohan Rao, Adsorption studies on treatment of textile dyeing industrial effluent by flyash, Chem. Eng. J., 116 (2006) 77–84.

[46] Y. Bulut, H. Aydin, A kinetics and thermodynamics study of methylene blue adsorption on wheat shells, Desalination, 194 (2006) 259–267.

[47] D. Kavitha, C. Namasivayam, Experimental and kinetic studies on methylene blue adsorption by coir pith carbon, Bioresour. Technol., 98 (2007) 14–21.

[48] A. Misra, R. Gupta, R.C. Gupta, Utilization of Marble Slurry in Construction Materials, in: Workshop on Gainful Utilization of Marble Slurry and Other Stone Waste, Indian School of Mines, Accessed, 2008.

[49] O. Acisli, I. Acar, A. Khataee, Preparation of a fly ash-based geopolymer for removal of a cationic dye: isothermal, kinetic and thermodynamic studies, J. Ind. Eng. Chem., 83 (2020) 53–63.